

Constraints on the Formation of the Globular Cluster IC 4499 from Multi-Wavelength Photometry*

A. R. Walker¹†, A. M. Kunder¹, G. Andreuzzi², A. Di Cecco³, P.B. Stetson⁴, M. Monelli⁵, S. Cassisi⁶, G. Bono³, R. De Propris¹, M. Dall’Ora⁷, J. M. Nemeč⁸, M. Zoccali⁹

¹*Cerro Tololo Inter-American Observatory, National Optical Astronomy Observatory, Casilla 603, La Serena, Chile*

²*Fundación Galileo Galilei - INAF, Breña Baja, La Palma, Spain*

³*Dipartimento di Fisica, Università di Roma Tor Vergata, via della Ricerca Scientifica 1, 00133, Rome, Italy*

⁴*Dominion Astrophysical Observatory, Herzberg Institute of Astrophysics, National Research Council, Victoria, British Columbia V9E 2E7, Canada*

⁵*IAC, Calle Via Lactea, E38200, La Laguna, Tenerife, Spain and Departamento de Astrofísica, Universidad de La Laguna, Tenerife, Spain*

⁶*INAF-Osservatorio Astronomica di Collurania, via M. Maggini, 64100 Teramo, Italy*

⁷*INAF-Osservatorio Astronomico di Capodimonte, via Moiarello 16, 80131, Naples, Italy*

⁸*Department of Physics & Astronomy, Camosun College, Victoria, British Columbia V8P 5J2, Canada*

⁹*Depto de Astronomia y Astrofísica, P. Universidad Católica, Casilla 306, Santiago 22, Chile*

accepted for publication, MNRAS, Mar 18, 2011

ABSTRACT

We present new multiband photometry for the Galactic globular cluster IC 4499 extending well past the main sequence turn-off in the U , B , V , R , I , and $DDO\ 51$ bands. This photometry is used to determine that IC 4499 has an age of 12 ± 1 Gyr and a cluster reddening of $E(B - V) = 0.22 \pm 0.02$. Hence, IC 4499 is coeval with the majority of Galactic GCs, in contrast to suggestions of a younger age. The density profile of the cluster is observed to not flatten out to at least $r \sim 800''$, implying that either the tidal radius of this cluster is larger than previously estimated, or that IC 4499 is surrounded by a halo. Unlike the situation in some other, more massive, globular clusters, no anomalous color spreads in the UV are detected among the red giant branch stars. The small uncertainties in our photometry should allow the detection of such signatures apparently associated with variations of light elements within the cluster, suggesting that IC 4499 consists of a single stellar population.

Key words: Galaxy: globular clusters: individual: IC 4499 stars: Hertzsprung-Russell and colour-magnitude diagrams

1 INTRODUCTION

Galactic globular clusters (GCs) are populous collections of old stars dating from the first few Gyr after the Big Bang. Because they typically consist of 10^5 to 10^6 stars, even short-lived evolutionary phases can be well populated. The wide range in metal abundances, as well as their extensive lifetimes, make globular clusters key ingredients in any explanation of the stellar and chemical evolution of our Galaxy. With few exceptions, GCs have long been thought to be excellent examples of single stellar populations (SSPs, Renzini

& Buzzoni 1986) that formed at about the same time as our Galaxy. However, many GCs show light element abundance spreads indicative of the presence of multiple (but nearly coeval) populations.

The main goal of this paper is to take a fresh look at IC 4499, a Galactic GC with a mass somewhat lower than those clusters that most often clearly exhibit complex photometric behavior. If lower mass clusters correspond more closely to single stellar populations than the highest mass clusters, then the interpretation of their presumably simpler histories may be critical in deciphering the early evolution of our Galaxy and its system of GCs. Although major HST programs such as Sarajedini (2007) are providing outstanding data sets for the nearby clusters, many of the lower mass clusters ($\sim 5 \times 10^4 M_\odot$) still lack definitive study. The very lowest mass clusters are not tractable to study

* Based in part on observations made with the European Southern Observatory telescopes obtained from the ESO/ST-ECF Science Archive Facility.
† E-mail: awalker@ctio.noao.edu

as they do not contain statistically significant numbers of stars in the various evolutionary phases. However, moderate mass clusters such as IC 4499 do contain sufficient stars for population analyses and are relatively numerous in our Galaxy. Any explanation of their properties should be consistent with the exotic behavior seen in the generally more massive clusters.

If observations in multiple photometric bands are available, strong constraints on the complexities of GCs can be made. We present deep multiband optical photometry of IC 4499 in the *U*, *B*, *V*, *R*, *I*, and *DDO* 51 bands, and take advantage of this wavelength range for a detailed analysis of potential multiple components in this GC.

IC 4499 is a little-studied cluster lying in the intermediate-outer halo, with basic parameters (Harris 1996, 2010), of $R_{GC} = 15.7$ kpc, $M_V = -7.33$, $[Fe/H] = -1.53$. It is a low-density cluster that allows ground-based studies to penetrate to the cluster center to below the main sequence (MS) turnoff, and is principally distinguished by its apparent relatively young age (Ferraro et al. 1995) and the large number of RR Lyrae variables it contains (Fourcade et al. 1974; Coutts 1975; Clement et al. 1979); it has the highest specific frequency (numbers normalized to mass) of RR Lyrae variables contained in any galactic GC listed by Harris (2010) with the exception of the low mass cluster Palomar 13. The variables have an Oosterhoff Type I (Oo I) period distribution (Oosterhoff 1939), and a substantial fraction are double-mode (RRd) oscillators, first studied by Clement et al. (1986). A comprehensive CCD study of the variable star population was made by Walker & Nemeč (1996).

From low-resolution spectroscopy of four red giant branch (RGB) stars, Russell Cannon, quoted in Sarajedini (1993), derived a mean metallicity $[Fe/H] = -1.65 \pm 0.10$, and this value was used in the first color magnitude diagram (CMD) study by Sarajedini (1993). A deeper CMD by Ferraro et al. (1995) found a best fit to the observations with an isochrone with age 11 Gyr, some 3 Gyr younger than the bulk of Galactic GCs on the age scale then employed.

There are two more recent studies of IC 4499. Storm (2004) derived the cluster distance from single-epoch K-band observations and the $M_K - \log P - [Fe/H]$ relation of Bono et al. (2003). Assuming $[Fe/H] = -1.65$, he found a distance $(m - M)_0 = 16.47 \pm 0.04$ (statistical) ± 0.06 (systematic). Finally, Hankey & Cole (2010) measured a precise metallicity of $[Fe/H] = -1.52 \pm 0.12$ for 43 radial-velocity selected IC 4499 members using AAOmega on the AAT.

Using the *B*, *V* and *I* passbands, new CMDs for IC 4499 are presented and interpreted. More than a decade has passed since the last CMD investigations of IC 4499, and in that time the age of the Universe has been refined by the WMAP experiment (Bennett et al. 2010); for a standard Λ CDM model the best-fit age is 13.7 Gyr. Formation of galaxies and the first Galactic GCs is expected to have happened relatively quickly, within approximately the first Gyr, by 12.8 ± 0.4 according to Marin-Franch et al. (2009). Modern isochrones (e.g. the BaSTI archive, available on-line at <http://www.oa-teramo.inaf.it/BASTI/>) are used here to investigate whether IC 4499 is a “young” GC with an age 2–4 Gyr younger than clusters of similar metallicity (Ferraro et al. 1995), and to provide an updated age determination of this cluster.

As the observations reach farther than the tidal radius of IC 4499, an investigation of a possible association of IC 4499 with extratidal stars is carried out. On the basis of its supposedly young age and position in the Galaxy, IC 4499 has been proposed to be associated with the Monoceros Ring, a structure whose interpretation is contentious (Hammersley & Lopez-Corredoira 2010) but most likely appears to be a tidal stream remnant of a galaxy that merged with our own (Grillmair 2006; Conn et al. 2008; Casertti-Dinescu et al. 2006; Chou et al. 2010). Recently, the radial velocity of IC 4499 was shown to be within the range of the halo GCs and not inconsistent with being associated with membership in the Monoceros Ring (Hankey & Cole 2010).

This paper is organized as follows: §2 is a description of the observational material, §3 is the presentation of the CMDs from which we estimate the structural parameters of the cluster, and compare them with theoretical isochrones from which the age, distance, and reddening are derived, §4 is a discussion of the radial stellar distribution of IC 4499, §5 describes a search for the existence of multiple stellar populations, and §6 is a summary of our conclusions.

2 OBSERVATIONS AND PHOTOMETRY

2.1 Observations

The CCD imaging observations used here include all the observations of IC 4499 obtained by Walker & Nemeč (1996, hereafter WN96) with various telescopes at CTIO over the period 1987–1996, and all publicly available IC 4499 data that we were able to locate; these images are now contained within a private archive maintained by PBS. Further observations were carried out specifically for this project in May 2008 using the Mosaic II Imager on the CTIO Blanco 4m telescope, and in April 2009 with IMACS on the 6.5m Magellan Baade. The data thus span a range from 1987 to 2009; in total, there are 1365 individual CCD images from 24 observing runs. A summary of these data is presented in Table 1.

2.2 Photometry

All observations were reduced using the DAOPHOT IV and ALLFRAME suite of programs (Stetson 1987, 1994). The photometry was calibrated to a standard photometric system, closely approximating Landolt (1992), using algorithms called CCDSTD, CCDAVE and NEWTRIAL. These are the modules that were used to produce the photometry discussed in Stetson (2000, 2005) and many other papers devoted to particular star clusters. Indeed, CCDSTD and CCDAVE have been used in essentially their current form for more than twenty years. NEWTRIAL is fundamentally the same program as was used in Stetson (1996) and most of the papers from the Hubble Space Telescope Key Project on the Extragalactic Distance Scale (see Freedman et al. 2001, and references therein). CCDSTD uses synthetic-aperture photometry of established photometric standard stars to derive transformation equations relating the observed instrumental magnitudes to the standard photometric system. CCDAVE employs these equations to calibrate the instrumental measurements of those standards and of selected, isolated stars

Table 1. IC 4499 Observations

Dates	Telescope	Detector	Images
1987 Feb 03-06	CTIO 0.9m CFIM	TI 800	6 B, 6 V, 5 R
1987 Mar 06-11	CTIO 0.9m CFIM	RCA 512x320	31 B, 32 V, 32 R
1987 Mar 29	CTIO 1.5m CFIM	TI 800	3 B, 3 V, 3 R, 2 I
1987 Apr 17	CTIO 0.9m CFIM	TI 800	1 B, 1 V
1987 Jun 05-11	CTIO 0.9m CFIM	TI 800	44 B, 44 V, 44 R
1988 Mar 23	CTIO 4.0m CFIM	TI 800	2 U, 2 B, 2 V
1988 Jul 10-11	CTIO 0.9m CFIM	TI 800	3 B, 3 V
1989 Apr 18	CTIO 0.9m CFIM	TI 800	7 B, 6 V
1990 Mar 22-24	CTIO 1.5m CFIM	TI 800	8 U, 47 B, 49 V
1990 Mar 24	CTIO 4.0m PFIM	TI 800	9 U, 11 B, 9 V
1990 Jun 20	CTIO 4.0m PFIM	TI 800	6 B, 2 V
1990 Jun 24-25	CTIO 1.5m CFIM	Tek 512	8 U, 36 B, 36 V
1992 Feb 18	CTIO 4.0m PFIM	Tek 2K	15 B, 19 V
1992 Jul 09	ESO NTT EMMI	Thomson 1K	7 B, 9 V, 6 R, 6 I
1992 Sep 19	ESO NTT EMMI	Thomson 1K	15 B, 15 V
1993 Mar 03	ESO NTT EMMI	Thomson 1K	9 B, 9 V
1993 Apr 29-30	ESO NTT EMMI	Tek 1K	18 B, 20 V, 2 R, 2I
1993 Jun 27-28	ESO NTT EMMI	Tek 1K	14 B, 15 V, 1 R, 1I
1994 Mar 07-11	CTIO 0.9m CFIM	Tek 2K	32 B, 32 V, 32 I
1994 Apr 26	CTIO 0.9m CFIM	Tek 2K	2 B, 2 V, 2 I
1994 Jun 27-28	CTIO 0.9m CFIM	Tek 2K	30 V
1996 Mar 10	CTIO 4.0m PFIM	Tek 2K	20 V, 30 I
2008 May 03	CTIO 4.0m Mosaic	SITe 2Kx4K	4 U, 6 B, 6 V, 4 I, 4 DDO51 ($\times 8$)
2009 Apr 03	Magellan 6.5m IMACS	SITE 2Kx4K	22 V, 16 I ($\times 8$)

that are intended to become local standards in the various target fields. Finally, NEWTRIAL uses the local standard stars and the transformation equations to calibrate the entire corpus of observations for all stars in a target field to the standard photometric system.

With these algorithms, it is possible to calibrate data obtained under either photometric or non-photometric (i.e., thin or scattered clouds) observing conditions. For a night when conditions were photometric, a full transformation solution is obtained for each filter with a form like:

$$v_{\text{observed}} = V_{\text{standard}} + \alpha_0 + \alpha_1 X + \alpha_2(B-V) + \alpha_3(B-V)^2$$

where v is the aperture-corrected instrumental magnitude resulting from the CCD measurement normalized for the integration time, X is the airmass, and V and $B-V$ are presumed known quantities from the literature. The α 's in the transformation equation are unknown quantities to be determined from the observations of photometric standard stars made during the night, and are obtained by application of a robust least-squares technique. The instrumental magnitude v has a measuring error associated with it, resulting from Poisson photon noise, readout noise, PSF-fitting uncertainties (if relevant) and uncertainties in the aperture correction.

In the corresponding transformation for B , the color-extinction term, $\alpha_4(B-V)X$ with α_4 usually equal to -0.016 is used. The U-band transformations incorporate terms $\alpha_2(U-B)$, $\alpha_3(B-V)$ and $\alpha_4(B-V)^2$ to deal with that awkward regime among the B-A-F stars where a single value of $U-B$ may be found in stars with three different values of $B-V$. Spatial terms α_5x and α_6y involving the (x, y) coordinates of the star within the digital CCD image are used for large-format CCDs and for mosaic cameras.

Observations made on non-photometric occasions can be used to reduce the random photometric errors among stars in a single target field, producing tighter sequences in color-magnitude and color-color diagrams. For images taken on non-photometric nights, no extinction correction or uni-

versal zero-point is derived. Instead, we use a transformation equation of this general form:

$$v_{\text{observed}} = V_{\text{standard}} + \zeta_i + \alpha_2(B-V) + \alpha_3(B-V)^2 + \dots$$

A unique zero-point, ζ_i , for each CCD image i is derived from standard stars contained within that image. The color-correction terms can be derived from CCD images containing multiple standard stars with a range of color and/or from observations made with the same equipment during photometric nights of the same observing run,

The program CCDAVE inverts the calibration equations: the instrumental magnitudes (e.g., v) are still regarded as observed quantities with associated observational standard errors; the α 's are now regarded as known constants; and the star's calibrated magnitude on the standard system V (etc.) is the unknown to be determined by a robust least-squares statistical adjustment. Statistical estimates of the single optimum values of the magnitudes in other bandpasses, such as U , B , R , and I are obtained in exactly the same way at the same time. Since standard-system colors must be known for the color terms of the various photometric transformation equations, determination of these standard-system magnitudes must be iterative in nature; a neutral color is initially assumed for the star and substituted into the various transformation equations associated with the different observations of it, and as estimates of the star's standard-system magnitudes improve, the color indices employed in the transformation equations are refined and the magnitudes are redetermined. The coefficients of the color terms are small—a few hundredths of a magnitude per magnitude for a filter that is a reasonable approximation to the standard bandpass—and the convergence to a satisfactory solution is almost never a problem.

CCDAVE can derive standard-system magnitudes for the standard stars exactly as it does for the target stars of unknown photometric properties. The inputs to the program are only the observed instrumental magnitudes and the transformation equations. CCDAVE has no prior knowledge of the standard photometric indices or, indeed, which stars

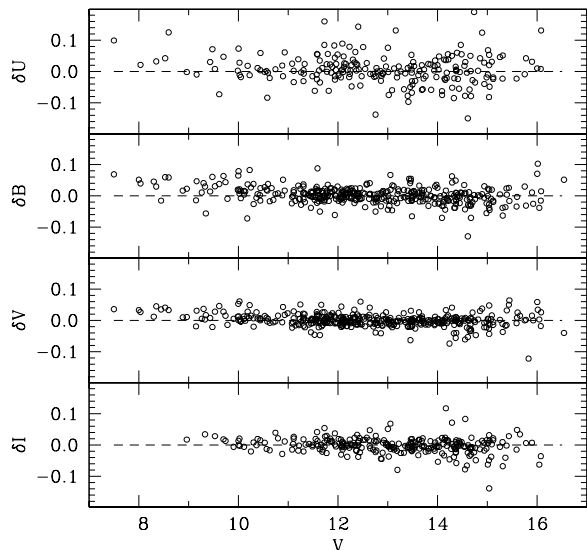


Figure 1. The difference in U , B , V , and I for stars in standard-system magnitudes and the stars obtained here, plotted against apparent visual magnitude. From 215 to 376 stars are plotted, depending upon the filter.

are standards and which are targets. A comparison between the output results for the standard stars produced by CCDAVE and the published values for the same stars that were used as input to CCDSTD, therefore, provides a clean test of the end-to-end validity of the methodology. As of the date of the submission of the revised version of this article, a total of 2,076 datasets have been homogeneously analyzed with CCDSTD and CCDAVE; among these are 263 that include observations of IC 4499.

Figure 1 and Figure 2 show the magnitude differences between the standard-system magnitudes produced by CCDAVE and the published values for the fundamental standard stars—those of Landolt (1973, 1983, 1992) and Graham (1981, 1982)¹. Figure 1 shows the magnitude residuals (in the sense published minus ours) plotted versus apparent visual magnitude, while Figure 2 plots the same residuals against $B-I$ color, serving as a proxy for effective temperature or, equivalently, spectral class. The stars shown here have been observed on a minimum of five photometric occasions, and have a standard error of the mean magnitude smaller than 0.02 mag. The weighted mean differences between the published results and ours are $+0.0035 \pm 0.0024$, $+0.0028 \pm 0.0011$, -0.0009 ± 0.0008 and -0.0009 ± 0.0012 mag in U , B , V , and I , respectively, based upon 215, 361, 376, and 253 stars. (For completeness, we report here a simi-

¹ Apart from modest additive zero-point adjustments, -0.002 ± 0.002 , -0.002 ± 0.001 , and -0.002 ± 0.001 in U , B , and V , respectively, to place the Landolt (1973) results on the same system as Landolt (1983, 1992), based upon 119 stars in common, we find no evidence within our data to suggest that these studies do not define the same photometric system, within the errors.

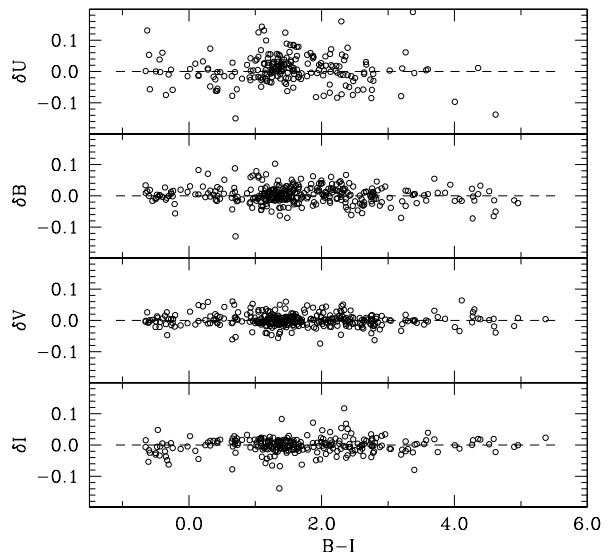


Figure 2. The difference in U , B , V , and I for stars in standard-system magnitudes and the stars obtained here, plotted against $(B - I)$ color.

lar difference of -0.0002 ± 0.0009 mag, based on 244 stars, in the R filter; the R band plays no role in our study of IC 4499.) Expressed as a standard deviation, the average standard residual of one star is 0.032, 0.020, 0.014, and 0.017 mag in U , B , V , and I . Together, these two figures demonstrate that our version of the standard photometric system matches the definitive published results for the same stars with a high degree of fidelity over a dynamic range of ~ 600 in flux ($9 \lesssim V \lesssim 16$) and over the full available range of temperature.

Considering now the observations of IC 4499, CCDSTD and CCDAVE are employed to define a sequence of local photometric standards in each target field of scientific interest, by transfer of photometric calibration from fundamental photometric standards in other parts of the sky. NEWTRIAL transfers the calibration to the complete set of instrumental magnitudes measured by the DAOPHOT/ALLFRAME suite of algorithms for all stars in a particular target field—in the present case, IC 4499. NEWTRIAL considers results from all observing nights and runs simultaneously. It assembles the totality of observed instrumental magnitudes for any given star, associates each measured instrumental magnitude with the transformation equation appropriate to the night, detector, filter, and image from which it was obtained, and uses a robust least-squares adjustment to estimate the single best mean magnitude in each photometric bandpass that optimally explains the corpus of observations in the corresponding filter.

Some exposures using the *DDO* 51 filter were also taken. Observations in this filter were standardized by using the approximation

$$DDO\ 51 = 0.67 * V + 0.33 * B$$

which was then used to define “standard” *DDO* 51 magnitudes for the local standard stars. Observed indices were fitted to these values in the usual way. Then we defined

$$\Delta = DDO\ 51 - 0.67 * V - 0.33 * B,$$

which is a good gravity-sensitive index for red stars, as clearly shown by (Teig 2008). In particular, *DDO* 51 can be useful in separating globular cluster Red Giant Branch (RGB) stars from foreground dwarfs.

Additionally we note that IC 4499 has a high southern declination and as a consequence its airmass as viewed from telescopes at the mid-latitude Chilean observatories is always rather high and nearly constant, ~ 1.8 – 2.0 . The cluster observations themselves cannot be used to self-calibrate extinction during a night’s observations, as its own extinction hardly changes.

We find significant offsets between the standardization performed here and reductions of the data presented by WN96. In particular, the following relations are found for 42 of 55 local standards from WN96:

$$\begin{aligned} V \text{ (here)} &= V \text{ (WN96)} + 0.042 \\ B \text{ (here)} &= B \text{ (WN96)} + 0.044 \\ I \text{ (here)} &= I \text{ (WN96)} + 0.017 \end{aligned}$$

and therefore:

$$\begin{aligned} (B - V) \text{ (here)} &= (B - V) \text{ (WN96)} + 0.002 \\ (V - I) \text{ (here)} &= (V - I) \text{ (WN96)} + 0.025 \\ (B - I) \text{ (here)} &= (B - I) \text{ (WN96)} + 0.027 \end{aligned}$$

We believe that the addition of extra observations on photometric nights and the use of vastly greater number of (secondary) photometric standards made in the present study has allowed a more accurate calibration. However, and importantly, the $B - V$ offset between the two studies is almost negligible, and so the extensive discussion on reddening in WN96 is still relevant. As photometry in the V , B , and I bands is more extensive than for the other bands, only the photometry in these filters will be used when calibration to a standard photometric system is of importance.

For each object the detected error, CHI of fit, and roundness parameter are used to help eliminate poorly measured stars, unresolved blends, and non-stellar objects. Intensity and magnitude mean magnitudes were calculated for the RR Lyrae using codes which fitted Fourier series to the data. The extensive IC 4499 RR Lyrae variable star observations have been combined with earlier photographic observations for a discussion of period changes in OoI and OoII clusters (Kunder et al. 2011).

3 C-M DIAGRAM OF IC 4499

3.1 Completeness

The fitting of theoretical isochrones to data requires a knowledge of the completeness of the star sample to avoid introducing any biases, particularly in the critical main sequence

turnoff (MSTO) region. The catalogue extends several magnitudes below the MSTO region. As there will be no discussion of the main sequence luminosity function, it is not necessary to perform a rigorous analysis at faint magnitudes. In particular, we remind the reader that our body of data consists of 1365 CCD images obtained with at least twelve different equipment setups on five different telescopes. The individual images were centered on many different locations within the cluster field, and the various images were subject to many different conditions of seeing, guiding, and sky brightness. Any given star can have as many as 357 observations in a single filter, or as few as one. To map out the detection completeness as a function of magnitude, color, and position on the sky would therefore be a prohibitively expensive endeavor. We thus map out the zone of magnitude/position space where completeness issues do not unduly complicate matters by a simpler and more approximate methodology.

The limits of sample completeness are estimated by considering the cluster luminosity function in a series of radial zones. These zones were chosen to cover the cluster extent, with roughly similar numbers of stars in each zone. It is presumed that the worst incompleteness will occur in the innermost zone, where the crowding is most severe, and possibly also in the outermost zone, where the total available exposure time is least.

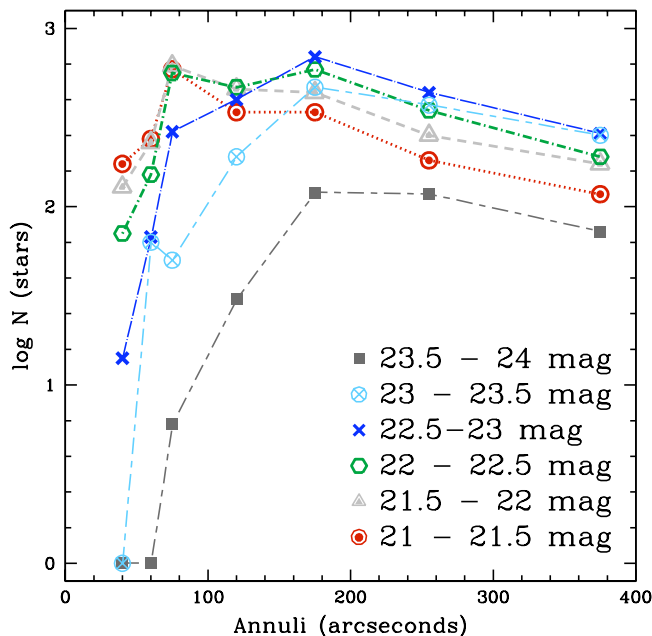
Our procedure is to plot the logarithm of the star counts against apparent magnitude. The luminosity functions of the outermost two zones are compared: over the magnitude range where they are closely parallel, it is presumed that both are comparably complete. Near the faint end, the apparent magnitude at which they begin to diverge is where one or the other is beginning to be incomplete. That done, the next zone—counting inward—is compared to the sum of the two outermost zones, and the magnitude extent over which the luminosity functions are closely parallel is again determined. Then the next radial zone is compared to the sum of the three outer zones, and so on. In this way, the apparent magnitude of incipient incompleteness as a function of radial distance from the cluster center is mapped. With this approach, as one moves inward, the magnitude range over which the luminosity functions may be compared becomes increasingly restricted as the onset of incompleteness moves brightward. At the same time, however, the star-counting statistics are improved, as each individual radial zone is compared to the sum of all zones lying farther from the cluster center.

Here 0.5 mag wide bins are chosen and a color range sufficient to contain the MS stars. The $V, V-I$ CMD is used, as this is deeper and tighter than the others, primarily due to the high-resolution Magellan data. Zones with differing radii are chosen (see Table 2), and the luminosity functions for the different zones are then slid until they overlap, starting with the outer zone then sliding and adding the inner zones one by one. These results are illustrated in Figure 3 and Table 2 where the columns contain (1) the radial zone and (2)–(5) the number of stars in each magnitude bin.

Because the completeness as a function of magnitude changes rapidly as one approaches the cluster center, we also experimented with zones of 30–50 arcsec and 50–70 arcsec. For the six zones constructed here the field star contamination is very small, and can be neglected. Furthermore, the

Table 2. Star Counts ($\log N$) as a function of V magnitude

Magnitude Annuli (arcsec)	21.0 - 21.5	21.5 - 22.0	22.0 - 22.5	22.5 - 23.0	23.0 - 23.5	23.5 - 24.0
0 - 50	2.42	2.26	1.95	1.26	0.30	0.0
50 - 100	2.77	2.79	2.75	2.42	1.70	0.78
100 - 140	2.53	2.66	2.67	2.60	2.28	1.48
140 - 210	2.53	2.64	2.77	2.84	2.67	2.08
210 - 300	2.26	2.40	2.54	2.64	2.57	2.07
300 - 450	2.07	2.24	2.28	2.41	2.40	1.86
30 - 50	2.24	2.11	1.85	1.15	0	0
50 - 70	2.38	2.36	2.18	1.83	1.80	0

**Figure 3.** *Left:* The number of stars per radial zone for IC 4499. The different symbols represent different magnitudes bins, which are specified in the bottom right corner.

completeness statistic for an ALLFRAME-produced catalogue remains close to 100% as the catalogue limit is approached and then rapidly falls to zero at fainter magnitudes, in contrast to a single reduction of stacked frames (cf., for instance, Stetson 1991). From Table 2, the $\sim 90\%$ completeness level is derived and shown in Table 3.

In conclusion, for our study of the populations of resolved stars brighter than the MSTO ($V \sim 20.5$) as a function of radius, outside a radius of 50 arcsec completeness corrections are negligible (Table 3). Hence, fitting isochrones to a similar sample should be safe. In principle, when fitting cluster observations with isochrones, it is not necessary for the sample to be complete, but that the sample is statistically significant. This is because the isochrones are fit to the shape of the CMD. The completeness is more important for star counts, LFs, and for the luminosity profile.

Table 3. V -band Magnitude Completeness Limits

Annuli (arcsec)	90% Limit
0-30	< 21.25
30-50	21.25
50-70	22.0
70-100	22.25
100-140	22.75
140-450	23.0

3.2 Reddening

IC 4499 is an outer halo cluster, one of 35 such according to the $R_{GC} > 15$ kpc definition of van den Bergh & Mackey (2004). With $(l, b) = (307^\circ.35, -20^\circ.47)$ we view the cluster on the far side of our Galaxy and through a considerable amount of dust. WN96 calculated the reddening for IC 4499 using four methods, two of these are dependent on the cluster metallicity for which they chose $[\text{Fe}/\text{H}] = -1.65$, and the other two involved colors of the RR Lyrae variables and the colors of the instability-strip boundaries. All methods were consistent, with the result $E(B - V) = 0.22 \pm 0.02$. To this we add the result from use of the Schlegel et al. (1998) reddening maps which show that a 5 arcmin radius centered on IC 4499 has $E(B - V) = 0.224 \pm 0.004$ (statistical). Regions centered approximately 15–20 arcmin N and S have slightly higher reddening, $E(B - V) \sim 0.24$ and 0.26 respectively, but elsewhere within 15 arcmin of the center of IC 4499 the reddening is within the range $E(B - V) = 0.21$ – 0.23 . Given the relatively small angular size of the cluster, there appears to be no need to apply variable reddening corrections, and indeed we do not find any evidence for their necessity. However small scale variations in reddening at the few percent level (~ 0.01 mag) cannot be ruled out. In summary, we find from the several methods available that $E(B - V) = 0.220 \pm 0.005$, where the error is derived from the scatter of the individual estimates. As systematic errors in the various calibrations likely dominate, we will adopt $E(B - V) = 0.22 \pm 0.02$.

In order to compare the observed CMD to isochrones, and to fit the CMD in colors other than $(B - V)$, we solve equations 1 and 3 of Cardelli, Clayton & Mathis (1989) for a variety of $R_V = A_V/E(B - V)$. For example, with $R_V = 3.1$ and $E(B - V) = 0.22$, $E(V - I) = 0.30$ whereas for $R_V = 3.3$ and $E(B - V) = 0.22$ then $E(V - I) = 0.31$ (here we assume that the I photometric band corresponds to an effective wavelength of 800 nm; cf. Kron, White & Gascoigne

1953; Cousins 1976; Landolt 1983). Within reasonable limits, R_V is an adjustable parameter. However in fitting the isochrones (see below) we found no reason not to choose $R_V = 3.1$.

3.3 CMDs of IC 4499

The CMD of IC 4499 is shown in Figure 4, with three different color baselines. The morphology has been described in previous investigations, with the exception that here the MS extends to $V \sim 24$ with high precision. The short horizontal branch is well populated in the region of the instability strip; hence many of these stars are RR Lyrae variables, marked by crosses in Figure 4. There is considerable contamination of the cluster RGB with field stars, due to the cluster position in the sky.

Figure 4 shows the BaSTI isochrones set with the following parameters: canonical, α -enhanced, $Z = 0.0006$, $[\alpha/\text{Fe}] = +0.4$, $[\text{M}/\text{H}] = -1.49$, $E(B - V) = 0.22$, $R_V = 3.1$, $\text{DM}_0 = 16.47$, and these isochrones are simultaneously fitted on the $V, B - V$, $V, B - I$ and $V, V - I$ CMDs. The ZAHB locus with these same parameters is also shown. Because the stellar models used in the present analysis do not account for the updated conductive opacities provided by Cassisi et al. (2007), a shift of $+0.05$ mag in V to the BaSTI ZAHB is applied as discussed by the quoted authors. We established the distance modulus by matching the isochrones to the horizontal branch stellar distribution, and find that it is identical to that found by Storm (2004). The metallicity is consistent with spectroscopy of RGB stars from Hankey & Cole (2010) from which the cluster metallicity was found to be $[\text{Fe}/\text{H}] = -1.52 \pm 0.12$. The α -element enhancement is assumed to be similar ($[\alpha/\text{Fe}] = +0.4$) to that for halo globular clusters in general.

The data shown in Fig. 4 reveals that theoretical isochrones with age 11 Gyr and 13 Gyr appear to properly bracket the cluster photometry. Therefore, we estimate an age of 12 ± 1 Gyr for IC 4499. It is worth noting that present result does not support the younger age of IC 4499 found by Ferraro et al. (1995) compared to the majority of Galactic GCs. On the contrary, our age is coeval with them (Marin-Franch et al. 2009).

The difference in the age estimate with respect to that of Ferraro et al. (1995), can be - at least partially - explained as a consequence of the use of a more updated and reliable theoretical framework. However, the use of a different, updated set of isochrones such as those provided by VandenBerg et al. (2000) and Dotter et al. (2007), does not affect our final cluster age determination. In fact, all state-of-the-art isochrones such as the BaSTI set give ages that are consistent with the WMAP age of the Universe of 13.7 Gyr (Bennett et al. 2010), and provide a quite similar age ranking for the Galactic GCs system (see, e.g. De Angeli et al. 2005; Marin-Franch et al. 2009; Cassisi et al. 2011, and references therein).

We emphasize that care must be taken when comparing relative ages with those in the older literature, as the range of ages for the majority group of older GCs with no age-metallicity relation is under 1 Gyr (Marin-Franch et al. 2009) compared to the several Gyr commonly proposed in the past, where uncertainties in the distance scale and magnitude-metallicity relation for RR Lyrae variables

propagated into the ages, as discussed for instance by Buonanno et al. (1989) and Walker (1992).

4 TIDAL RADIUS AND EXTRA-TIDAL STARS

There is increasing evidence that some globular clusters now part of our Galactic GC system formed in dwarf galaxies that subsequently—over a Hubble time—merged with our own Galaxy, with the present-day merger example of the Sagittarius dwarf and its central GC M54 and other associated clusters being a case in point (Bellazzini et al. 2008; Carretta et al. 2010a). Several GCs have been associated with stellar streams in the Galactic halo that are presumably remnants of earlier mergers, e.g. NGC 5053 (Lauchner et al. 2006), NGC 5466 (Grillmair & Johnson 2006) and Terzan 5 (Ferraro et al. 2009; Origlia et al. 2010), while others are surrounded by extra-tidal stars e.g., NGC 1851 and NGC 1904 (Olszewski et al. 2009; Carballo-Bella & Martinez-Delgado 2010) or distinct tidal tails such as that for Palomar 5 (Odenkirchen et al. 2009; Rockosi et al. 2002) indicating ongoing dynamical evolution. In a spectroscopic survey of a limited number of giant candidates in the IC 4499 field, Hankey & Cole (2010; also Hankey 2011, private communication) found several stars that appear to share the cluster’s radial velocity despite lying more than 24 arcminutes from the cluster center.

The tidal radius of IC 4499 was determined to be 12.35 arcmin by Trager, Djorgovski & King (1995). The structural parameters for most of the clusters included in Trager, Djorgovski & King (1995) were derived via surface-brightness measurements from photographic plates and/or small-format CCD images, after manual removal of areas affected by stars believed to belong to the foreground. In the case of IC 4499 alone, the cluster profile was derived via numerical differentiation of previously published photoelectric photometry; the authors do not mention any correction for field-star contamination for this cluster. Due to its location in the sky, $(l^{II}, b^{II}) = (307, -20)$, IC 4499 is unfortunately seen through a fairly rich Galactic foreground: simulated star counts from the Besançon model (Robin et al. 2003) (see particularly their Fig. 6) predict approximately 3000 field stars per square degree with V brighter than 20 mag. Most of these stars are expected to have colors similar to the RGB and the turnoff region.

Our data for IC 4499—which appear to be appreciably better than any that were previously available—extend to a maximum distance of 33 arcmin from the cluster center, and we have complete coverage out to a distance of 14 arcmin. Therefore we should be able to derive an independent and possibly more definitive measure of the cluster’s tidal radius than has hitherto-fore been possible.

We have experimented with a new methodology for distinguishing the cluster density profile from foreground-field contamination, which we will describe here in some detail. We begin by identifying an “acceptance region” or “box” in the color-magnitude plane where the vast majority of cluster members are found. Our assumption will be that the number of true cluster members falling outside the acceptance region will be small compared to those inside. The number of field stars contained within the acceptance box may be small, relative to the number falling outside it, but we do

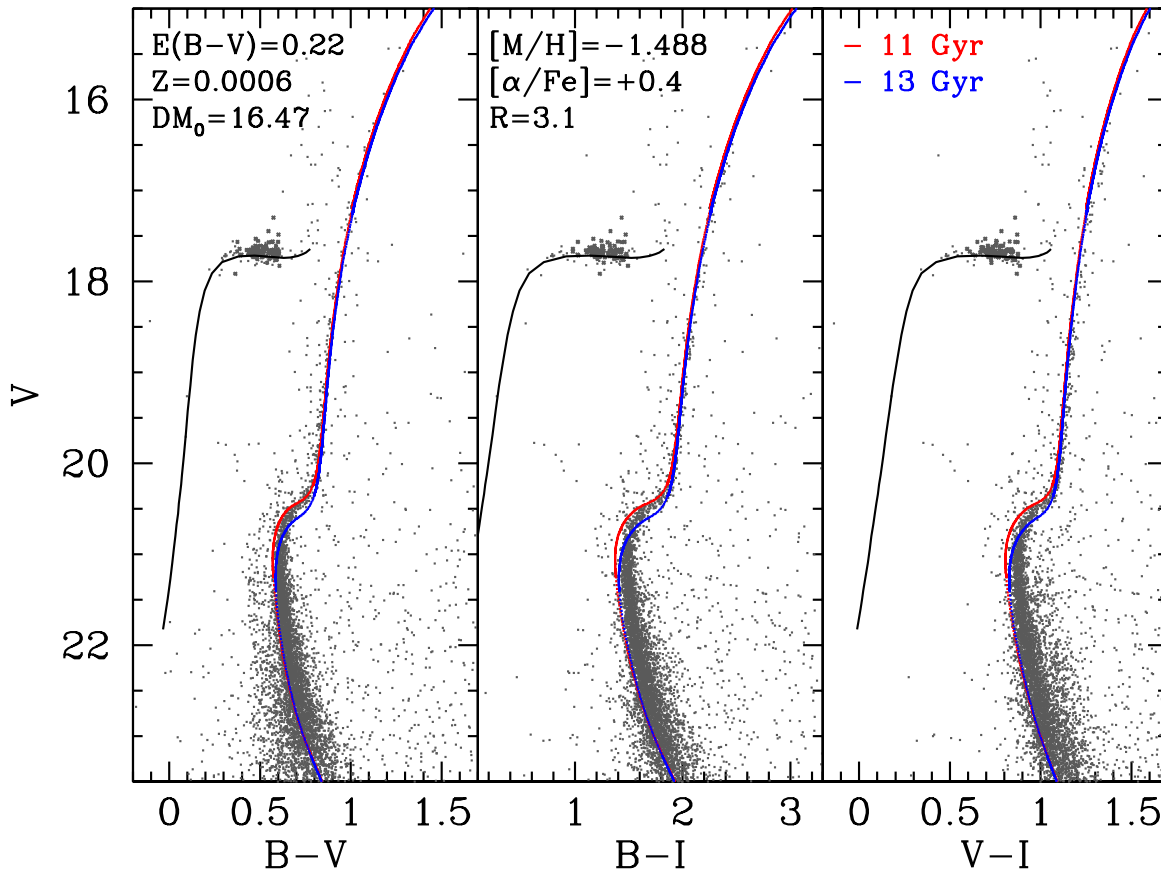


Figure 4. IC 4499 Color Magnitude Diagrams to the $V, B-V$ CMD (left), $V, B-I$ CMD (center) and $V, V-I$ CMD (right) are shown. Over-plotted are isochrones from the BaSTI database and correspond to canonical, α -enhanced calculations for ages of 11 and 13 Gyr, with other parameters as displayed on the plots. The RR Lyrae variables are designated by crosses.

not expect that number to be negligible. We will, however, assume that neither the cluster population nor the field population changes significantly with position within our overall field of view. The surface density of field stars falling outside the box in the CMD will be easy to estimate quantitatively, because we expect contamination of this sample by cluster stars to be small and—in particular—negligible at large distances from the cluster. We will then examine the ratio of star counts *inside* the acceptance region to counts *outside* the acceptance region as a function of distance from the cluster center. We will take the asymptotic limit of this ratio at large radial distance as representing the number ratio of field stars inside the box to field stars outside the box. The surface density of field stars inside the box thus derived can then be subtracted from the radial profile of star counts to yield the decontaminated cluster profile.

To isolate that part of the color-magnitude diagram where cluster members dominate, we plotted the stars with the smallest intrinsic photometric errors lying within the annulus $10'' \leq r \leq 180''$ centered on the cluster (see Figure 5). A cubic spline was fitted to the cluster ridge line and an acceptance region was defined where the majority of cluster stars are found to lie. The left panel of Figure 6 displays

the $V, B-I$ CMD of the entire sample of stars with no selection in radial distance and with a very mild selection in photometric error ($\sigma_{BVI} \leq 0.25$ mag). The solid line shows the ridge line, while the dashed ones display the acceptance region. This box has a width in color of 0.01 mag close to the tip of the Red Giant Branch (RGB) and increases to 0.3 mag at magnitudes fainter than the main sequence turn-off (MSTO). At visual magnitudes fainter than 22.75 mag, the acceptance region stops because the photometric errors increase and the ridge line is less accurate.

Using a $V, B-I$ CMD has the advantage of incorporating three independent measurements, thus limiting the possible occurrence of spurious detections. Further, $B-I$ colors have a stronger sensitivity to the effective temperature when compared with $B-V$ and $V-I$ colors, and in turn give a more robust estimate of the ridge line.

The middle panel of Figure 6 shows the cluster HB stars as well as the stars located inside the acceptance region. The candidate IC 4499 stars in the acceptance region encompass a rather generous color range, since a fraction of them might be affected by differential reddening. The right panel of Figure 6 shows the CMD of candidate field stars (rejected) with their typical peak in color around $(B-I) = 1.8-2$ mag. The

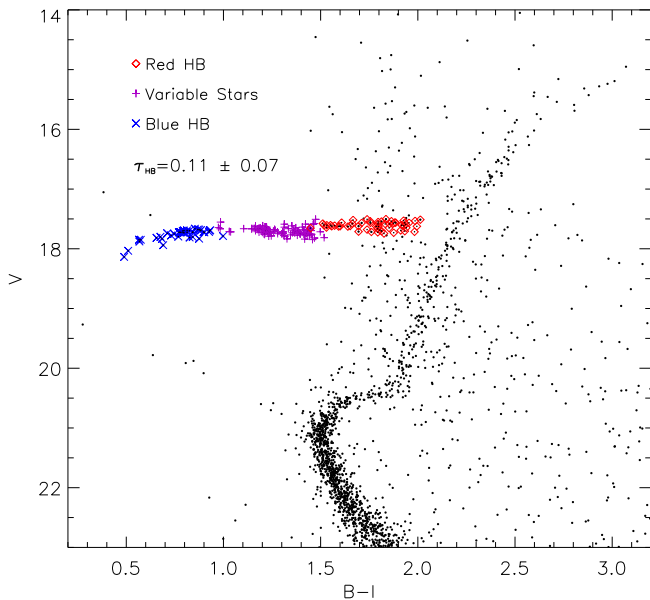


Figure 5. The IC 4499 $V, B - I$ Color Magnitude Diagram in which only stars with small photometric errors and within $10'' \leq r \leq 180''$ are plotted.

group of stars located at $V \sim 20$ and $(B-I) \sim 1$ includes cluster blue stragglers (BSs) and also chance optical blends of stars in the crowded regions of the cluster. Note that we do not count these among the cluster stars, which will result in a (very) minor underestimate of the number of true cluster members in the innermost one or two radial bins. This will have no significant effect whatsoever on our inferences for the outer part of the cluster profile. The BSs will be included in a study of the IC 4499 RRL and SX Phe stars by Nemec et al (in preparation).

With the acceptance region defined, we can now consider the radial density profiles of the “accepted” and the “rejected” stars. The center of the cluster lies some 887 arcseconds from the eastern edge of our survey area, 1386 arcseconds from the west edge, 842 arcseconds from the north edge, and 1508 arcseconds from the south edge. Therefore, we have a complete star sample only out to a radius of 842 arcseconds or 14 arcminutes; from 14 to 34 arcminutes we have a representative but incomplete sample. Accordingly, the field is divided into concentric annuli with an outermost limit at $r \sim 800''$; this is slightly larger than the aforementioned estimate of the tidal radius of the cluster.

The top panel of Figure 7 shows the logarithmic density of the number of “rejected” stars $-\ln[N_R]$ per arcmin²) as a function of the inverse of the radial distance. True cluster members that happen to lie within the rejection region of the CMD should represent a minor source of contamination in this plot, becoming negligible at large distances (small values of $\frac{1}{r_g}$). The middle panel of the figure shows the number ratio of stars in the box (N_A) to stars outside the box as a function of the inverse radial distance. Note that we can extend this curve to greater radial distances from the cluster ($\frac{1}{r}$ more closely approaching zero) than in the

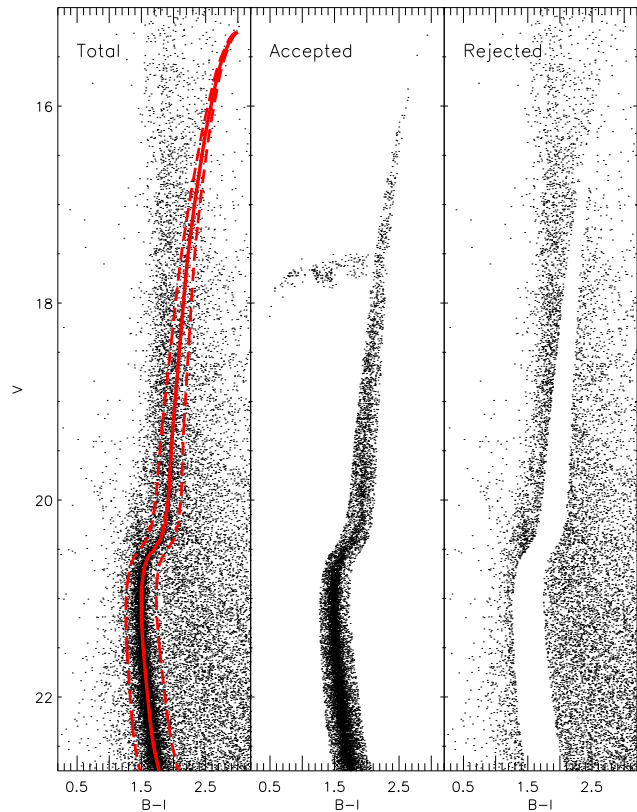


Figure 6. *Left:* The defined acceptance region for IC 4499 cluster members is shown with all observed stars from our stellar catalogue over-plotted. *Middle:* Only the candidate IC 4499 cluster members are shown. *Right:* The probable IC 4499 field stars are shown.

upper panel because stars in the corners of the study area, outside the fully sampled concentric annuli, can be used; the incomplete sampling at the larger distances complicates the calculation of surface densities, but does not affect the ratio of simple star counts. We estimate that the log of the ratio of field stars in the box to those outside the box approaches an asymptotic value of -0.80 ± 0.01 . The top panel of Fig. 4 indicates that the logarithm of the surface density of *field stars* in the *rejection region* of the CMD is 1.0 ± 0.02 . Combined, these numbers yield a total surface density of 11.6 stars per square arcminute: 10 stars per square arcminute fall outside the acceptance region in the CMD, and 1.6 stars per square arcminute fall inside the box.

The bottom panel of Figure 7 shows the density profile of the cluster with the number of spuriously accepted stars subtracted off. Because the radial profile is not observed to flatten at the largest distances, we conclude that the tidal radius of this cluster might be larger than previously estimated. Alternatively, we may be seeing evidence of a cluster halo, as has been suggested for M92 (by Testa et al. 2000; Lee et al. 2003; Di Cecco et al. 2009) and NGC 1851 (Olzowski et al. 2009). In a forthcoming investigation, we plan

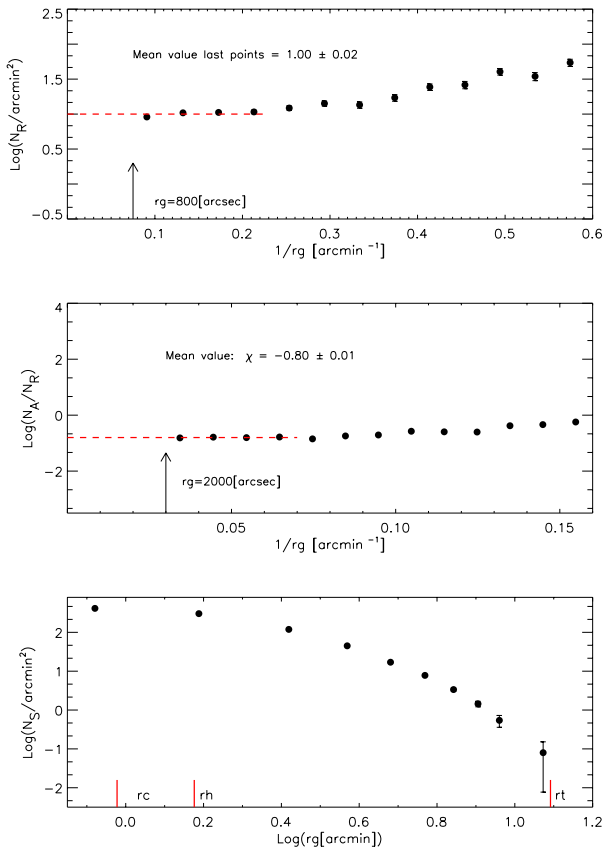


Figure 7. *Top:* The logarithmic density of the candidate field stars is plotted as a function of the inverse of the radial distance. *Middle:* The ratio between the number of accepted (N_A) and the number of rejected (N_R) stars, N_A/N_R , as a function of the inverse of the radial distance. *Bottom:* The density profile of the cluster with the number of spuriously accepted stars subtracted off. Note the very different ranges of radial distance shown in the three panels.

to perform a more detailed fit of the density profile to constrain the possible occurrence of a halo around IC 4499 and, in particular, whether the distribution of the outermost stars is azimuthally symmetric.

5 MULTIPLE POPULATIONS IN IC 4499

It is now known that many GCs contain more than one stellar generation (e.g., Piotto 2009 for a review). This manifests itself as abundance anomalies on the red giant branch, such as the CH/CN dichotomy and the O/Na, Mg/Al anticorrelations, indicating that the stellar material has been polluted with material released by a previous generation of stars (Carretta et al. 2010b).

However, it is possible to detect the presence of multiple population via U band imaging (e.g. Marino et al. 2008; Han et al. 2009; Kravtsov et al. 2010a,b; Lardo et al. 2011) as the CN and CH molecular features ‘line blanket’ this bandpass and therefore CH/CN strong giants will appear redder in a $U - (\text{optical})$ color-magnitude diagram. For example, Yong et al. (2008) showed that the Strömgen u traces the differ-

ences in N abundances for the stars of NGC 6752. Marino et al. (2008) showed that the RGB stars in M4 have a bimodal spread in a U vs. $(U - B)$ CMD, where the red side of the RGB is confirmed spectroscopically to be Na-poor and CN-weak and the bluer stars are Na-rich and CN-strong. Carretta et al. (2010b) showed that Na abundance is correlated with the spread in $(U - B)$ among RGB stars in NGC 3201. Lardo et al. (2011) showed that for the M5 stars, the Na-poor and Na-rich stars, which are tightly aligned along the narrow cluster RGB in the g vs. $(g - r)$ CMD, are clearly separated into two parallel sequences in the much broader giant branch seen in the g vs. $(u - g)$ diagram. The Na-rich stars appear systematically redder than Na-poor ones.

These results show that U photometry is a powerful diagnostic of light-element abundance spread; a spread in the UV – optical color on the RGB that is not seen in the optical – optical color is evidence of light-element variation in RGB stars. Similarly, the DDO 51 filter contains numerous Mg features, including the prominent MgH indices, and therefore scatter in this filter is sensitive to the Mg abundance variations known to be a marker of the presence of secondary stellar populations. Here the U band and DDO 51 band of the giant branch are used to check for possible signs of multiple populations in IC 4499.

We will first consider the sample of giant branch stars from Hankey & Cole (2010) in a recent spectrographic survey of giants in a 2° field around IC 4499. Of the 43 stars found to be probable cluster members, 42 had good photometry in our catalog. Figure 8 shows the $B, B - V$, $B, U - B$, and $B, B - DDO 51$ CMDs of these stars. Although this is a relatively small sample of stars, it has the advantage of being a decontaminated and unbiased giant sample. Following the Lardo et al. (2011) recipe for searching for bi-modality, a ridge line following the curvature of the observed RGB in $B, B - V$, $B, U - B$, and $B, B - DDO 51$ and located approximately at the red edge of the RGB, is taken as a reference to compute color spreads. The ridge line adopted is a 4th order polynomial that closely follows the theoretical RGB from the BaSTI models.

To take into account potential photometric errors that could affect the color spread, the bottom panel of Figure 9 shows the normalized color spread ($\Delta'_{col} = \Delta_{col} / \sigma_{col}$), the color spread of each star divided by the associated photometric uncertainty. The photometric error estimates are based on the root-mean-square agreement of the actual observations. There are 24 different telescope-CCD-filter combinations and dozens of observations per star. Hence, the photometric errors will be appropriate.

The wings of the Δ'_{col} distributions roughly coincide, and the core of the $B - V$ distribution is more peaked than its $U - B$ counterpart. This was observed for the different GCs studies by Lardo et al. (2011), but using the SDSS passbands and attributed to the spread in the abundance of light elements such as C, N, O, Na, etc.

As shown by Lardo et al. (2011), comparing Δ'_{col} distributions can reveal whether there is any significant spread in the $B, U - B$ red giant branch in addition to that due to photometric errors. As the U band is sensitive to CN and CH molecular features in giant stars, a spread in $B, U - B$ compared to $B, B - V$ can be attributed to variations in CN/CH line strengths in the giants.

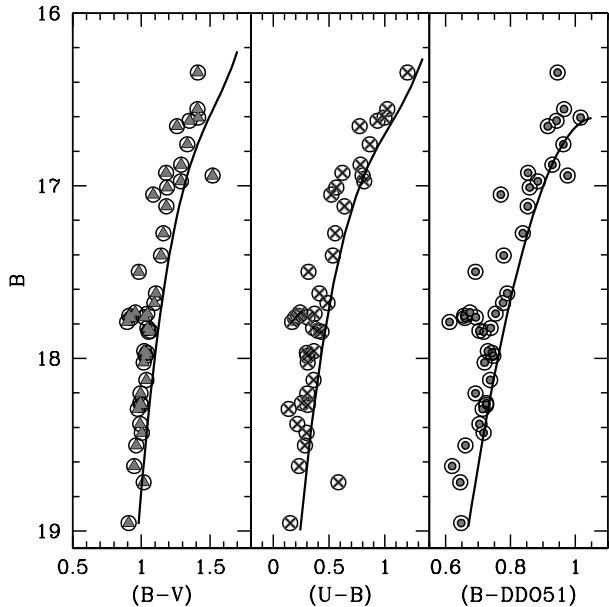


Figure 8. The B , $(B-V)$, B , $(U-B)$ and B , $(B-DDO51)$ CMDs for 42 giant stars in IC 4499. The curves approximately tracing the red edges of the RGBs are used as references to compute the color spread distributions shown in Figure 9.

This same process is repeated for $\Delta'_{(B-DDO51)}$, to exploit the sensitivity of the DDO51 filter to Mg indices.

To establish whether the $B-V$ and $U-B$ or the $B-V$ and $B-DDO51$ distributions are different (and to what degree of significance), we carried out a Kolmogorov-Smirnov test. Several iterations of the KS test were run and the value of the shift that maximizes the probability that the two samples are drawn from the same parent population, P_{KS}^{phot} , is found (Lardo et al. 2011). This ensures that only the shape of the distributions between $\Delta'_{(B-V)}$ and $\Delta'_{(U-B)}$ is considered, and not potential unphysical shifts from, *e.g.*, the way the ridge line is defined (and hence Δ'_{col}). The $\Delta'_{(B-V)}$ and $\Delta'_{(U-B)}$ samples cannot be distinguished at a 93% confidence level. Similarly, the $\Delta'_{(B-V)}$ and $\Delta'_{(B-DDO51)}$ color spreads cannot be distinguished at an 80% confidence level. These results are summarized in Table 4.

The KS test indicates that the color distributions shown in Figure 9 have the same shape. However, it does not test whether the shapes are due to the same stars or completely different stars which have color distributions that produce a similar spread. Figure 10 shows a positive, linear correlation for $\Delta'_{(B-I)}$ versus $\Delta'_{(U-B)}$, $\Delta'_{(B-V)}$ and $\Delta'_{(V-I)}$. This is strong evidence that the color-spread is intrinsic in Δ'_{col} and includes a significant component of temperature spread in not only the $(U-B)$, but also the $(B-V)$ and $(V-I)$. Hence, the $\Delta'_{(U-B)}$, $\Delta'_{(B-V)}$ and $\Delta'_{(V-I)}$ distributions all have a range

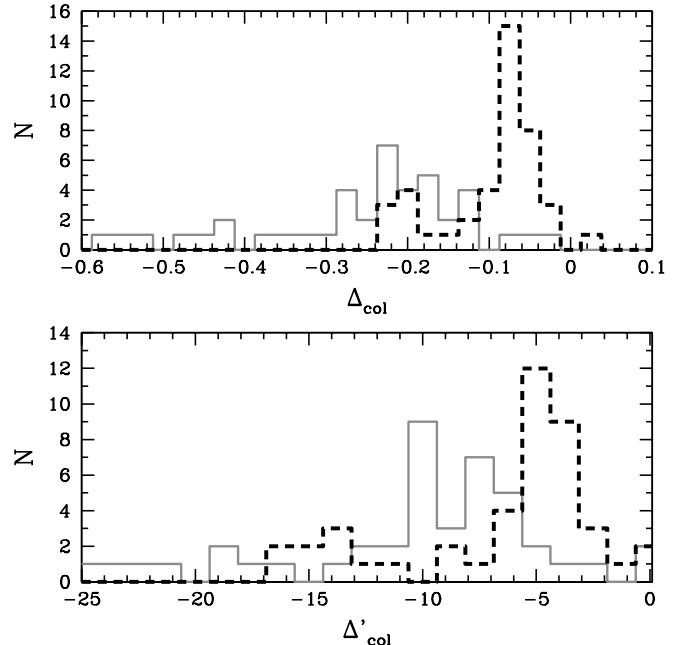


Figure 9. *Top:* The color spread with respect to the RGB fiducials for the $(B-V)$ (dashed histogram) and $(U-B)$ (solid histogram) distributions. *Bottom:* Same as above, but the color spread has been normalized to take into account photometric errors.

Table 4. Results of KS tests

Color distribution	P_{KS}^{phot}	$P_{KS,all}^{phot}$
$\Delta'_{(U-B)}$	0.93	0.58
$\Delta'_{(B-DDO51)}$	0.80	0.90

of temperatures at fixed apparent magnitude. This indicates that there is no spread in UV color on the RGB that is not seen in the optical.

To increase the sample size, we will now consider giant stars selected using the DDO 51 filter in a similar procedure outlined by Teig (2008). Figure 11 shows a color-color plot in $V-I$, $DDO51-V$ of all stars in the red giant magnitude range ($B < 20$ mag). Over-plotted are the confirmed cluster members from Hankey & Cole (2010) as well as the stars shown to have radial velocities and metallicities that are not consistent with IC 4499 membership. The polynomial fits used by Teig (2008) to separate M33 giants and dwarfs are also shown, where the polynomial is shifted to account for the reddening of the cluster. Probable giant candidates are chosen as stars within 0.01 mag of the polynomial that represents the giants, and that have $DDO51-V > 0.9$ mag.

Using these giant candidates, a KS test is run between the $\Delta'_{(B-V)}$ and $\Delta'_{(U-B)}$ distributions. The two samples cannot be distinguished at a 58% confidence level. Between the $\Delta'_{(B-V)}$ and $\Delta'_{(B-DDO51)}$ distributions, $P_{KS,all}^{phot}$ is 90%. Again these results are detailed in Table 4.

Using the U, B, V, I and $DDO51$ passbands, no evidence for an anomalous color spread along the giant branch is seen

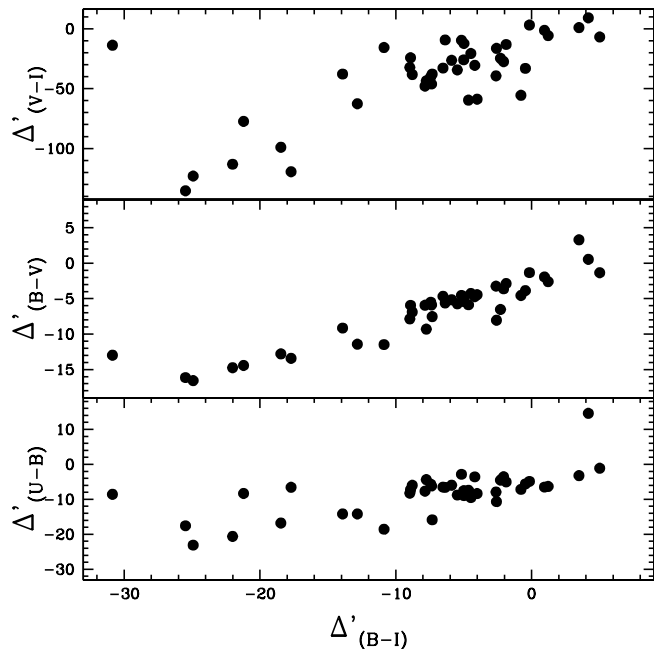


Figure 10. The $\Delta'_{(B-I)}$ versus $\Delta'_{(U-B)}$, (bottom panel), $\Delta'_{(B-V)}$, (middle panel), and $\Delta'_{(V-I)}$ (top panel).

for IC 4499. This result is in contrast to the more massive GCs studied by Lardo et al. (2011). The photometry presented here not only has photometric uncertainties quite a bit smaller than the photometry used by Lardo et al. (2011)—the Δ'_{col} distributions are ~ 4 times more sensitive, but also the multiple passbands allow for a greater variety of color spreads to be detected. Still, no anomalous color spread along the RGB is seen.

If the anomalous color spread is due to variations in the abundances of light elements, this effect would be weaker for lower metallicities. Hence, for GCs like IC 4499, (clusters with $[\text{Fe}/\text{H}] > -1.7$ dex) this method may not be able to detect anomalous color spreads. On the other hand, Lardo et al. (2011) was able to detect an anomalous color spread in M15 ($[\text{Fe}/\text{H}] \sim -2.26$), M53 ($[\text{Fe}/\text{H}] \sim -1.99$) and M92 ($[\text{Fe}/\text{H}] \sim -2.28$), which are substantially more metal-poor than IC 4499.

Therefore the absence of an anomalous color spread implies that any multiple stellar populations in IC 4499 must have smaller differences in the light elements compared to more massive GCs in which color spreads were detected using near ultraviolet bands. This is in agreement with the general idea that low-mass GCs do not have a deep potential well. A deep potential well would allow the retention of ejecta of first generation stars and increase the chance of forming a second star generation (D’Ercole et al. 2008). If this behavior is found for other medium-mass GCs as well, then that would imply that lower-mass GCs have simpler histories.

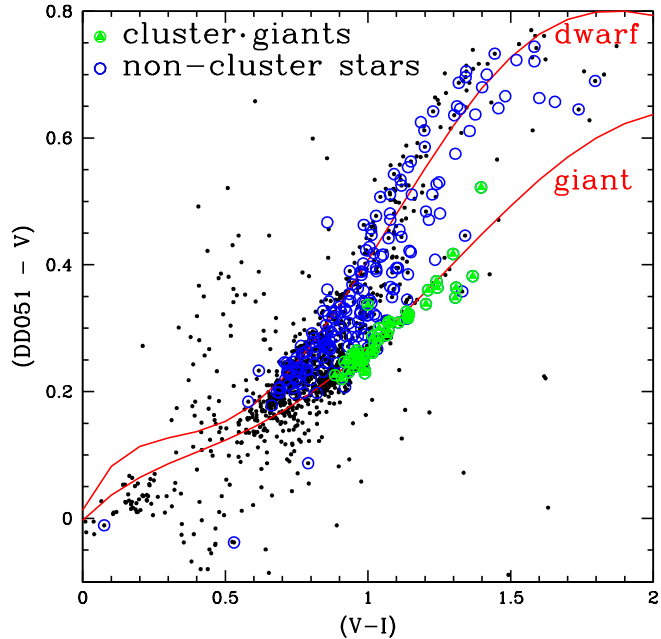


Figure 11. The $(DDO51 - V)$, $(V - I)$ color-color plot used to select giant candidates in IC 4499. The green symbols represent cluster giants confirmed spectroscopically by Hankey & Cole (2010), whereas the blue symbols represent stars that Hankey & Cole (2010) found are not consistent with IC 4499 cluster membership. Polynomial fits used by Teig (2008) to separate M33 giants and dwarfs are also shown in red.

6 CONCLUSIONS

We present new U , B , V , R , I , and $DDO\ 51$ photometry of the Galactic globular cluster IC 4499. As the multiband photometry extends well below the main sequence turn-off, current BaSTI isochrones are fitted to three color baselines to derive an age of 12 ± 1 Gyr. This is the first modern age estimate for IC 4499. Despite previous suggestions of a younger age for IC 4499 (Ferraro et al. 1995), we find that IC 4499 is coeval with them the majority of Galactic GCs.

The density profile of the cluster is measured to search for signs of tidal streams and/or extra-tidal stars. Out to $r \sim 800''$, the density profile continues to change. This could be because the tidal radius is larger than previously estimated. It could also be that IC 4499 is surrounded by a halo, similar to that claimed for M92 (Testa et al. 2000; Lee et al. 2003; Di Cecco 2009) and in NGC 1851 by Olszewski et al. (2009). More wide-field data is needed to constrain the radial extent of IC 4499.

A search for possible multiple components in IC 4499 is carried out. Using U , B , V , I , and $DDO\ 51$, and 43 red giant branch stars confirmed spectroscopically by Hankey & Cole (2010), no anomalous color spreads potentially due to variations in the abundances of light elements are detected. To increase the sample size, the $DDO\ 51$ narrow band filter is used to select a sample of 100 probable giants. Also with this sample, no anomalous color spread is detected. This is in contrast to the more massive GCs studied by Lardo et al. (2011), in which different components using near ultraviolet bands were detected. Given the small photometric errors

in our catalog, this implies a rather small spread of light elements among the giant branch stars in IC 4499.

ACKNOWLEDGMENTS

This research has made use of the NASA/IPAC Extragalactic Database (NED) which is operated by the Jet Propulsion Laboratory, California Institute of Technology, under contract with the National Aeronautics and Space Administration. AdC, GB and SC have been partially supported by PRIN INAF 2009 (PI. Prof. R. Gratton). MM is funded by the IAC (grant P3/94) and by the Science and Technology Ministry of the Kingdom of Spain (grant AYA2007-3E3507).

REFERENCES

- Bellazzini, M. et al. 2008, *AJ*, 136, 1147
 Bennet, C. et al. 2010, arXiv1001.4758
 Bono, G. et al. 2003, *MNRAS*, 344, 1097
 Buonanno, R., Corsi, C. & Fusi Pecci, F. 1989, *A&A*, 218, 80
 Carballo-Bella, J.A. & Martinez-Delgado, D. 2010, Highlights of Spanish Astrophysics V, *Astrophys. & Space Science Proceedings*, Springer-Verlag, p. 383
 Cardelli, J., Clayton, G. & Mathis, J. 1989, *ApJ*, 345, 245
 Carretta, E., Bragaglia, A., Gratton, R., & Lucatello, S. 2009, *A&A*, 505, 139
 Carretta, E., Bragaglia, A., Gratton, R., Lucatello, S., Bellazzini, M., & D’Orazi, V. 2010a, *ApJ*, 712, 21
 Carretta, E., Bragaglia, A., Gratton, R. G., et al. 2010b, *A&A*, 516, A55
 Casetti-Dinescu, D. et al. 2006. *AJ*, 132, 2082
 Cassisi, S., Potekhin, A.Y., Pietrinferni, A., Catelan, M. & Salaris, M. 2007, *Apj*, 661, 1094
 Cassisi, S., Marín-Franch, A., Salaris, M., Aparicio, A., Monelli, M., & Pietrinferni, A. 2011, *A&A*, 527, 59
 Chou, M-Y, Majewski, S., Cunha, K, Smith, V., Patterson, R. & Martinez-Delgado, D. 2010. arXiv 1007.1056
 Clement, C., Dickens, R.J. & Bingham, E.E. 1979, *AJ*, 84, 217
 Clement, C., Nemeč, J.M., Robert, N., Wells, T., Dickens, R.J. & Bingham, E.A. 1986, *AJ*, 92, 825
 Conn, B.C. et al. 2008. *MNRAS*, 390, 1388
 Conroy, C. & Spergel, D. 2010, arViv 1005.4934
 Cousins, A.W.J. 1976, *Mem. R. Astron. Soc.*, 81, 25
 Coutts, C., Dickens, R.J., Epps, E. & Read, M. 1975, *ApJ*, 1971, 45
 D’Antona, F. & Caloi, V. 2008, *MNRAS*, 390, 693
 De Angeli, F., Piotto, G., Cassisi, S., Busso, G., Recio-Blanco, A., Salaris, M., Aparicio, A., & Rosenberg, A. 2005, *AJ*, 130, 116
 Denissenkov, P & Weiss, A. 2004, *ApJ*, 603, 119
 D’Ercole, A., D’Antona, F., Ventura, P., Versperini, E., McMillan, S. 2010, *MNRAS*, 407, 854
 D’Ercole, A., Versperini, E., D’Antona, F., McMillan, S. & Recchi, S. 2008, *MNRAS*, 391, 825
 Di Cecco et al. 2009, *MmSAI*, 80, 81
 Dotter, A., Chaboyer, B., Jevremović, D., Baron, E., Ferguson, J.W., Sarajedini, A., & Anderson, J. 2007, *AJ*, 134, 376
 Eggen, O., Lynden-Bell, D., & Sandage, A. 1962, *ApJ*, 136, 748
 Ferraro, I., Ferraro, F.R., Pecci, F. Fusi, Corsi, C.E. & Buonanno, R. 1995, *MNRAS*, 275, 1057
 Ferraro, F.R. 2009, *Nature*, 462, 1028
 Fourcade, C.R., Laborde, J.R. & Arias, J.C. 1974, *A&AS*, 18, 3
 Freedman, W. L., et al. 2001, *ApJ*, 553, 47
 Graham, J. A. 1981, *PASP*, 93, 29
 Graham, J. A. 1982, *PASP*, 94, 244
 Gratton, R., Sneden, C. & Carretta, E. 2004, *ARAA*, 42, 385
 Gratton, R., D’Orazi, V., Bragaglia, A., Carretta, E. & Lucatello, S., 2010, *A&A*, 522, 77
 Grillmair, C.J. 2006, *ApJ*, 651, 29
 Grillmair, C.I. & Johnson, R. 2006, *ApJ*, 639, 17
 Hammersley, P. L. & Lopez-Corredoira, M. 2010, arXiv1011.2405
 Han, S., Lee, Y., Joo, S., et al. 2009, *ApJ*, 707, L190
 Hankey, A.J. & Cole, A.A. 2010, *MNRAS*, in press
 Harris, W.E. 1996, *AJ*, 112, 1487
 Harris, W.E. 2010, arXIV: 1012.3224v1
 Kravtsov, V., Alcaíno, G., Marconi, G., & Alvarado, F. 2010a, *A&A*, 512, L6
 Kravtsov, V., Alcaíno, G., Marconi, G., & Alvarado, F. 2010b, *A&A*, 516, A23
 Kron, G.E., White, H.S., & Gascoigne, S.C.B. 1953, *ApJ*, 118, 502
 Kunder, A. et al. 2011, *AJ*, 141, 15
 Landolt, A.U. 1973, 78, 959
 Landolt, A.U. 1983, *AJ*, 88, 439
 Landolt, A.U. 1992, *AJ*, 104, 340
 Lardo, C., Bellazzini, M., Pancino, E., Carretta, E., Bragaglia, A., & Dalessandro, E. 2011, *A&A*, 525, 114
 Lauchner, A., Powell, W.L., & Wilhelm, R. 2006, 651, 33L
 Lee, Y-W., Joo, J-M, Sohm, Y-J, Rey, S-C, Lee, H-C, Walker, A. 1999, *Nature*, 402, 55
 Lee, K.H., Lee, H.M., Fahlman, G.G., & Lee, M.G. 2003, *AJ*, 126, 815
 Maeder, A. & Meynet, G. 2006, *A&A*, 448, 37
 Marin-Franch, A. et al. 2009, *ApJ*, 694, 1498
 Marino, A. F., Villanova, S., Piotto, G., et al. 2008, *A&A*, 490, 625
 de Mink, S.E., Pols, O.R., Langer, N. & Izzard, R.G. 2009, *A&A*, 507, L1
 Mucciarelli, A. et al. 2010, *MNRAS*, in press
 Muratov, A. L. & Gnedin, O. Y. 2010, *ApJ*, 718, 1266
 Odenkirchen, M., Grebel, E., Kayser, A., Rix H-W, Dehnen, W. 2009, *AJ*, 137, 3378
 Olszewski, E., Saha, A., Knežek, P., Subramaniam, A, de Boer, T., Seitzer, P. 2009, *AJ*, 138, 157
 Oosterhoff, P.T. 1939, *Observatory*, 62, 104
 Origlia, L. et al., 2010, arXiv1012.2047
 Pancino, E., Ferraro, F., Bellazzini, M., Piotto, G. Zoccali, M. 2000, *ApJ*, 534, 83
 Piotto, G. 2009. *Proc. IAUS* 258, 233
 Renzini, A. 2008, *MNRAS*, 391, 354
 Renzini, A. & Buzzoni, A. 1986, *ASSL*, 122, 195
 Robin, A.C., Reylé, C., Derrière, S. & Picaud, S. 2003, *A&A*, 409, 523
 Rockosi, C. et al. 2002, *AJ*, 124, 349
 Sarajedini, A. 1993. *AJ*, 105, 2172

- Sarajedini, A. 2007, IAUS 241, 218
Schlegel, D., Finkbeiner, D. & Davis, M. 1998, ApJ, 500, 525
Stetson, P.B. 1987, PASP, 99, 191
Stetson, P.B. 1991, in *The Formation and Evolution of Star Clusters*, ASP Conf. Ser. 13, ed. K. Janes (ASP: San Francisco), p. 88
Stetson, P.B. 1994, PASP, 106, 250
Stetson, P. B. 1996, PASP, 108, 851
Stetson, P.B. 2000, PASP, 112, 925
Stetson, P.B. 2005, PASP, 117, 563
Storm, J. 2004, A&A, 415, 987
Teig, M. 2008, PASP, 120, 474
Testa, V., Zaggia, S. R., Andreon, S., Longo, G., Scaramella, R., Djorgovski, S. G., & de Carvalho, R. 2000, A&A, 356, 127
Trager, S., Djorgovski, S. & King, I. 1995. AJ, 109, 218
VandenBerg, D.A., Swenson, F.J., Rogers, F.J., Iglesias, C.A., & Alexander, D.R. 2000, ApJ, 532, 430
van den Bergh, S. & Mackey, A. 2004. MNRAS, 354, 713
Walker, A.R. 1992, ApJ, 390, L81
Walker, A.R. & Nemec, J.M. 1986, AJ, 112, 2026, WN96
Yong, D., Grundahl, F., Johnson, J. A., & Asplund, M. 2008, ApJ, 684, 1159